

OSCAR-based Reconstruction for Compressed Sensing and Parallel MR Imaging

L. El Gueddari ^{1,2}, P. Ciuciu^{1,2}, E. Chouzenoux ^{3,4}, A. Vignaud ¹ and J.-C. Pesquet³

¹CEA/NeuroSpin, Gif-sur-Yvette, France ²INRIA-CEA Saclay Ile-de-France, Parietal team, Univ Paris-Saclay, France ³CVN, Centrale-Supélec, Univ. Paris-Saclay, France ⁴LIGM, Paris-Est University, France

ISMRM 2019, Montreal, CAN



Outline

- 1 Motivation & Context
 - Why non-Cartesian acquisition
 - Non-Cartesian MR image reconstruction in parallel imaging
- 2 Calibration-less MR image reconstruction
 - Problem statement
 - Joint sparsity regularization
- 3 Experiments & Results
 - Experimental set-up
 - Results
- 4 Conclusion & Outlook

Anatomical MRI

Anatomical MRI is generally acquired using Cartesian sampling.

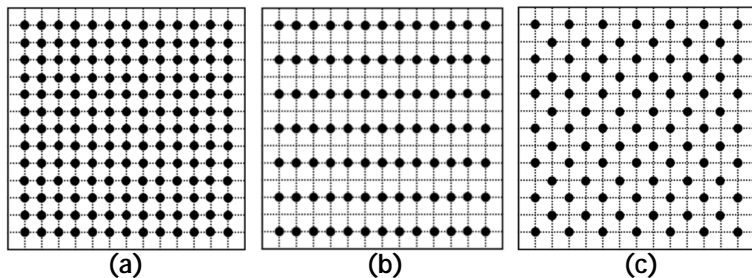


Figure: Typical (a) Cartesian (b) parallel acquisition (c) CAIPIRINHA¹ acquisition

... however in some cases non-Cartesian trajectories are useful ...

¹Breuer et al. 2006, *Magnetic Resonance in Medicine*.

Non-Cartesian trajectories for anatomical MRI

A non-exhaustive list of usages

- For ultra-short echo time imaging²
- X-nuclei imaging (TPI³)
- To correct for motion, especially for abdominopelvic MRI⁴

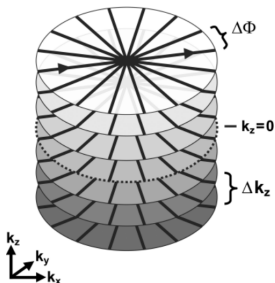


Figure: Stack of stars used for VIBE acquisition

²Johnson et al. 2013, *Magnetic Resonance in Medicine*.

³Boada et al. 1997, *Magnetic Resonance in Medicine*.

⁴Chandarana et al. 2014, *European radiology*.

Non-Cartesian trajectories for anatomical MRI

A non-exhaustive list of usages

- For ultra-short echo time imaging²
- X-nuclei imaging (TPI³)
- To correct for motion, especially for abdominopelvic MRI⁴

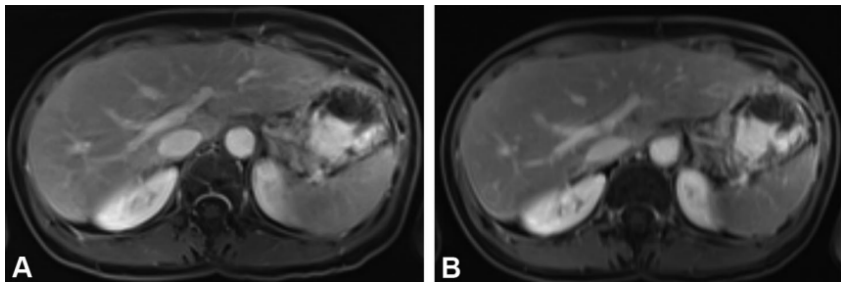


Figure: A: Free-breathing stack-of-stars VIBE, B: Breath-holding conventional VIBE

²Johnson et al. 2013, *Magnetic Resonance in Medicine*.

³Boada et al. 1997, *Magnetic Resonance in Medicine*.

⁴Chandarana et al. 2014, *European radiology*.

Non-Cartesian trajectories for anatomical MRI

Renewed interest to speed-up acquisition in the context of Compressed Sensing⁵.

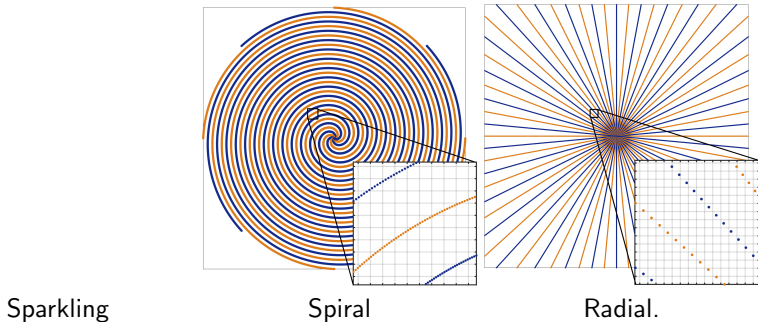


Figure: Example of non-Cartesian trajectories.

⁵Lazarus et al. 2019, *Magnetic Resonance in Medicine*.

Non-Cartesian trajectories for anatomical MRI

Renewed interest to speed-up acquisition in the context of Compressed Sensing

Figure: Comparison of different acquisition trajectories with 16-fold accelerated acquisition on T2*-weighted images.

⁵Lazarus et al. 2019, Magnetic Resonance in Medicine

Non-Cartesian trajectories for anatomical MRI

Parallel imaging acquisition: collect multiple k-space data using a multi-receiver coil as the latter is known to boost the SNR.

Illustration of multi-receiver coil (phased array).

How do we reconstruct MR images from non-Cartesian k-space measurements in parallel imaging?

Non-Cartesian MR image reconstruction in parallel imaging

Self-calibrating methods

Non-Cartesian reconstruction techniques can be split in two categories:

Self-calibrating methods:

⁷Samsonov et al. 2004, Magnetic Resonance in Medicine

⁸Uecker et al. 2014, Magnetic Resonance in Medicine

Non-Cartesian MR image reconstruction in parallel imaging

Self-calibrating methods

Non-Cartesian reconstruction techniques can be split in two categories:

Self-calibrating methods:

require a region where the signal has been sampled at least at the Nyquist rate

⁷Samsonov et al. 2004, Magnetic Resonance in Medicine

⁸Uecker et al. 2014, Magnetic Resonance in Medicine

Non-Cartesian MR image reconstruction in parallel imaging

Self-calibrating methods

Non-Cartesian reconstruction techniques can be split in two categories:

Self-calibrating methods:

require a region where the signal has been sampled at least at the Nyquist rate
model the coil sensitivity profiles S_c for all channels $c = 1; \dots; L$ ^{7;8}

⁷Samsonov et al. 2004, Magnetic Resonance in Medicine

⁸Uecker et al. 2014, Magnetic Resonance in Medicine

Non-Cartesian MR image reconstruction in parallel imaging

Self-calibrating methods

Non-Cartesian reconstruction techniques can be split in two categories:

Self-calibrating methods:

require a region where the signal has been sampled at least at the Nyquist rate
model the coil sensitivity profiles S_l for all channels $l = 1, \dots, L$ ^{7,8}
solve an inverse problem and recover a single full FOV image:

$$\mathbf{x} = \arg \min_{\mathbf{x} \in \mathbb{C}^N} \frac{1}{2} \sum_{l=1}^L \|\mathbf{y}_l - S_l \mathbf{x}\|_2^2 + \|\mathbf{x}\|_1 \quad (1)$$

$\mathbf{y}_l \in \mathbb{C}^M$ the l -th channel-specific data set

$\mathbf{x} \in \mathbb{C}^N$ the reconstructed image (ex. $N = 512 \times 512$)

F is the forward under-sampling Fourier operator

$\mathbf{K} \in \mathbb{C}^{N \times N}$ linear operator related to a sparse decomposition

⁷Samsonov et al. 2004, Magnetic Resonance in Medicine

⁸Uecker et al. 2014, Magnetic Resonance in Medicine

Non-Cartesian MR image reconstruction in parallel imaging

Self-calibrating methods

Non-Cartesian reconstruction techniques can be split in two categories:

Self-calibrating methods:

require a region where the signal has been sampled at least at the Nyquist rate
model the coil sensitivity profiles S_l for all channels $l = 1, \dots, L$ ^{7,8}
solve an inverse problem and recover a single full FOV image:

$$\mathbf{x} = \arg \min_{\mathbf{x} \in \mathbb{C}^N} \frac{1}{2} \sum_{l=1}^L \|\mathbf{F}_l \mathbf{S}_l \mathbf{x} - \mathbf{y}_l\|_2^2 + \lambda \|\mathbf{x}\|_1 \quad (1)$$

$\mathbf{y}_l \in \mathbb{C}^M$ the l -th channel-specific data set

$\mathbf{x} \in \mathbb{C}^N$ the reconstructed image (ex. $N = 512 \times 512$)

\mathbf{F} is the forward under-sampling Fourier operator

$\mathbf{S}_l \in \mathbb{C}^M \times \mathbb{C}^N$ linear operator related to a sparse decomposition

Note: Extraction of coil sensitivity maps is challenging in non-Cartesian cases

⁷Samsonov et al. 2004, Magnetic Resonance in Medicine

⁸Uecker et al. 2014, Magnetic Resonance in Medicine

Non-Cartesian MR Image reconstruction from multi-channel array coil acquisition

Calibration-less methods

Non-Cartesian reconstruction techniques can be split in two categories:

Calibration-less methods:

do not require any calibration region

⁹Trzasko and Manduca 2011, Signals, Systems and Computers (ASILOMAR), 2011
Conference Record of the Forty Fifth Asilomar Conference on

¹⁰Majumdar and Ward 2012, Magnetic Resonance in Medicine

Non-Cartesian MR Image reconstruction from multi-channel array coil acquisition

Calibration-less methods

Non-Cartesian reconstruction techniques can be split in two categories:

Calibration-less methods:

- do not require any calibration region

- solve an inverse problem but recover channel-specific images

⁹Trzasko and Manduca 2011, Signals, Systems and Computers (ASILOMAR), 2011
Conference Record of the Forty Fifth Asilomar Conference on

¹⁰Majumdar and Ward 2012, Magnetic Resonance in Medicine

Non-Cartesian MR Image reconstruction from multi-channel array coil acquisition

Calibration-less methods

Non-Cartesian reconstruction techniques can be split in two categories:

Calibration-less methods:

- do not require any calibration region

- solve an inverse problem but recover channel-specific images

- use the redundant information given by each coil to impose constraints such as

- low-rank CLEAR⁹ or group-sparsity CALM¹⁰

⁹Trzasko and Manduca 2011, Signals, Systems and Computers (ASILOMAR), 2011
Conference Record of the Forty Fifth Asilomar Conference on

¹⁰Majumdar and Ward 2012, Magnetic Resonance in Medicine

Non-Cartesian MR Image reconstruction from multi-channel array coil acquisition

Calibration-less methods

Non-Cartesian reconstruction techniques can be split in two categories:

Calibration-less methods:

- do not require any calibration region

- solve an inverse problem but recover channel-specific images

- use the redundant information given by each coil to impose constraints such as

- low-rank CLEAR⁹ or group-sparsity CALM¹⁰

- more likely to be used for on-line image reconstruction

⁹Trzasko and Manduca 2011, Signals, Systems and Computers (ASILOMAR), 2011
Conference Record of the Forty Fifth Asilomar Conference on

¹⁰Majumdar and Ward 2012, Magnetic Resonance in Medicine

Problem statement

Calibration-less MR image reconstruction problem solved using analysis formulation:

Definition

MR image reconstruction is formulated as follows:

$$\underline{x} = \arg \min_{\underline{x} \in \mathbb{C}^N} \frac{1}{2} \sum_{l=1}^L \|\mathbf{F}_l \underline{x} - \mathbf{y}_l\|_2^2 + g(\mathbf{T} \underline{x}) ; \quad (2)$$

with:

$\mathbf{y}_l \in \mathbb{C}^M$ the l^{th} channel-specific data set

$\mathbf{x} \in \mathbb{C}^N$ the l^{th} channel-specific reconstructed image ($N = 512 \times 512$)

\mathbf{F} is the forward under-sampling Fourier operator

$\mathbf{T} \in \mathbb{C}^{N \times N}$ linear operator related to a sparse decomposition

g is a convex regularization term that promotes sparsity

Optimization algorithm

Primal dual optimization

We aim to find:

$$\min_{\underline{x} \in \mathbb{C}^{N \times L}} [f(\underline{x}) + g(T\underline{x})] \quad (3)$$

where:

f is convex, differentiable on $\mathbb{C}^{N \times L}$ and its gradient is L -Lipschitz
 $g \in \Gamma_0(\mathbb{C}^{N \times L})$ ¹¹ with a closed form proximity operator, given by:

$$\text{prox}_g(\underline{z}) = \arg\min_{\underline{v} \in \mathbb{C}^{N \times L}} \frac{1}{2} \|\underline{z} - \underline{v}\|_2^2 + g(\underline{v}) \quad (4)$$

Note: Those are standard assumptions in optimization based image reconstruction methods.

¹¹ Γ_0 is the set of convex proper lower semi-continuous functions on $\mathbb{C}^{N \times L}$ taking values on $\mathbb{R} \cup \{\infty\}$

Optimization algorithm

Condat-Vu sequence

Using a primal-dual optimization method proposed by Condat¹², Vu¹³:

Algorithm 1: Condat-Vu algorithm

```

initialize  $k = 0$ ,  $\alpha > 0$ ,  $\beta > 0$ ,  $\underline{x}_0$ ,  $\underline{z}_0$ ;
while  $k < K$  do
     $\underline{x}_{k+1} := \underline{x}_k + \alpha (\text{r f}(\underline{x}_k) + \text{T} \underline{z}_k)$ ;
     $\underline{w}_{k+1} := \underline{z}_k + \beta \text{T} \underline{x}_{k+1} - \underline{x}_k$ ;
     $\underline{z}_{k+1} := \underline{w}_{k+1} - \text{prox}_{g= \frac{\beta}{2} \|\cdot\|_{\text{T}}^2}(\underline{w}_{k+1})$ ;
end

```

with:

the algorithm weakly converges to the solution of Eq. (3) if

$$\frac{1}{\alpha} - \beta \|\text{T}\|^2 > \frac{1}{2}$$

and hyper-parameters set as follows: $\alpha := \frac{1}{2\|\text{T}\|^2}$, $\beta := \frac{1}{2\|\text{T}\|^2}$

¹²Condat 2013, Journal of Optimization Theory and Applications.

¹³Vu 2013, Advances in Computational Mathematics.

Joint sparsity regularization

Group-LASSO

Parallel imaging has been proved to have tighter recovery guarantees than single channel acquisition when combined with Group-LASSO (GL) regularization¹⁴

Definition

The group-LASSO penalty is defined as follows:

$$g_{GL}(\underline{z}) = \sum_{s=1}^S \lambda \sqrt{p_s} \left\| \sum_{t=1}^T X_{st}^{-1} z_{sp} \right\|_2$$

λ and p_s are positive hyper-parameters
 p_s models the scale or subband dependence

¹⁴Chun, Adcock, and Talavage 2016, IEEE Transactions on Medical Imaging
For $p_s = 1$ the algorithm corresponds to Majumdar and Ward, Magnetic Resonance in Medicine, 2012

Joint sparsity regularization

Sparse group-LASSO

Variant: Sparse group-LASSO¹⁶ (sGL)

Definition

$$\forall \underline{z} \in \mathbb{C}^N; g_{\text{sGL}}(\underline{z}) = g_{\text{GL}}(\underline{z}) + \lambda \|\underline{z}\|_1 \quad (5)$$

being positive hyper-parameter.

sGL proximity operator¹⁸ is closed form and corresponds to the composition of GL proximity operator with soft-thresholding.

¹⁶Friedman, Hastie, and Tibshirani 2010, arXiv preprint arXiv:1001.0736.

Joint sparsity regularization

Octagonal Shrinkage and Clustering Algorithm for Regression

Inferring the structure via a pairwise ℓ_1 norm.
 OSCAR regularization¹⁷ is defined as follows:

Definition

$$g_{\text{OSCAR}}(z) = \sum_{s=1}^S \sum_{j=1}^L |z_{sj}| + \sum_{j < k} \max_j |z_{sj}|; |z_{sk}|$$

$$= \sum_{s=1}^S \sum_{j=1}^L (|z_{sj}| + 1) |z_{sj}| \quad (6)$$

where:

$z_{\#} \in \mathbb{R}^{N \times L}$ the wavelet coefficients sorted in decreasing order, i.e. $|z_{s1}| \geq |z_{s2}| \geq \dots \geq |z_{sL}|$.

α and β are some positive hyper-parameters that need to be set

Figure: Original wavelet coefficients (WC)

¹⁷Bondell and Reich 2008, Biometrics.

Joint sparsity regularization

Octagonal Shrinkage and Clustering Algorithm for Regression

Inferring the structure via a pairwise ℓ_1 norm.

OSCAR regularization¹⁷ is defined as follows:

Definition

$$g_{\text{OSCAR}}(z) = \sum_{s=1}^S \sum_{j=1}^{2^s} \lambda_{s,j} |z_{s,j}| + \sum_{j < k} \max\{|z_{s,j}|, |z_{s,k}|\} \quad (6)$$

where:

$\underline{z}_{\#} \in \mathbb{C}^N$ the wavelet coefficients sorted in decreasing order, i.e. $\lambda_{s,j} = \lambda_{s, P_s(j)}$.

and $\lambda_{s,j}$ are some positive hyper-parameters that need to be set

Figure: Sorted out WC in descending magnitude order

¹⁷Bondell and Reich 2008, Biometrics.

Joint sparsity regularization

Octagonal Shrinkage and Clustering Algorithm for Regression

Inferring the structure via a pairwise ℓ_1 norm.

OSCAR regularization¹⁷ is defined as follows:

Definition

$$g_{\text{OSCAR}}(z) = \sum_{s=1}^S \sum_{j=1}^L |z_{sj}| + \sum_{j < k} \max_j |z_{sj}|; |z_{sk}|$$

$$= \sum_{s=1}^S \sum_{j=1}^L (|z_{sj}| + 1) |z_{sj}| \quad (6)$$

where:

$z_{\#} \in \mathbb{C}^{N \times L}$ the wavelet coefficients sorted in decreasing order, i.e. $s \in \{1, \dots, N\}; |z_{s1}| \geq \dots \geq |z_{sP_s}|$.

α and β are some positive hyper-parameters that need to be set

Figure: Thresholded sorted WC

¹⁷Bondell and Reich 2008, Biometrics.

Joint sparsity regularization

Octagonal Shrinkage and Clustering Algorithm for Regression

Inferring the structure via a pairwise ℓ_1 norm.

OSCAR regularization¹⁷ is defined as follows:

Definition

$$g_{\text{OSCAR}}(z) = \sum_{s=1}^S \sum_{j=1}^L |z_{sj}| + \sum_{j < k} \max_j |z_{sj}|; |z_{sk}|$$

$$= \sum_{s=1}^S \sum_{j=1}^L (|z_{sj}| + 1) |z_{sj}| \quad (6)$$

where:

$z_{\#} \in \mathbb{R}^{N \times L}$ the wavelet coefficients sorted in decreasing order, i.e. $|z_{s1}| \geq |z_{s2}| \geq \dots \geq |z_{sL}|$.

α and β are some positive hyper-parameters that need to be set

Figure: Unsorting WC to their original position

¹⁷Bondell and Reich 2008, Biometrics.

Experimental set-up

Sequence parameters:

Ex-vivo baboon brain

7T Siemens Scanner GRE

1Tx/32Rx Nova coil

Sparkling trajectory

390 m 390 m in plane-resolution

3mm slice thickness

Acceleration factor of 15 in time

Under-sampling factor of 2.5

T: Undecimated Bi-Orthogonal 7-9 wavelet transform

Figure: Sparkling trajectory

Hyper-parameters set using a grid-search procedure.

Cartesian scan 512512 was acquired and used for reference.

Results

Quantitative assessment

Coil combination: Square root of the Sum-Of-Squares
Structural SIMilarity Index (SSIM)¹⁸ used to set hyper-parameters

Table: Image quality assessment for all regularizers.

	SSIM	pSNR (dB)	NRMSE
IFT	0.847	26.50	0.263
GL	0.864	26.92	0.254
sGL	0.851	26.77	0.259
OSCAR	0.875	30.49	0.177
ℓ_1 -ESPIRiT	0.874	28.32	0.238

Note: ℓ_1 -ESPIRiT is a self-calibrating method.

¹⁸Wang et al. 2004, IEEE transactions on image processing

Results

Comparison of the Sum-Of-Squares

Reference

IFT

GL

sGL

OSCAR

ℓ_1 -ESPIRiT

Results

Quantitative assessment

Comparison between coil images:

Figure: Assessment of the SSIM score per channel.

Results

Quantitative assessment

Comparison between coil images:

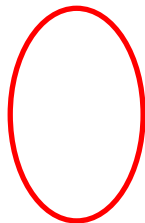


Figure: Assessment of the SSIM score per channel.

Results

Comparison of the image channels: low-SNR channel

No reg.
SSIM= 0:630

Group-LASSO
SSIM= 0:680

Sparse GL
SSIM= 0:672

OSCAR
SSIM= 0:646

Results

Quantitative assessment

Comparison between coil images:



Figure: Assessment of the SSIM score per channel.

Results

Comparison of the image channels: high-SNR channel

No reg.
SSIM= 0:846

Group-LASSO
SSIM= 0880

Sparse GL
SSIM= 0863

OSCAR
SSIM= 0893

Conclusion & Outlook

Conclusion:

- New parallel CS-MRI reconstruction algorithm

- No sensitivity maps

- OSCAR outperforms group-LASSO and sparse group-LASSO

- OSCAR and ℓ_1 -ESPIRiT are comparable, however the latest is self-calibrating

- Same optimization method to solve calibration-less MR reconstruction

Perspectives:

- Extension to 3D-MRI

- Study motion impact on the reconstruction

Code is available on GitHub: [LElGueddari/pysap/calibrationless_mri_reconstruction](https://github.com/LElGueddari/pysap/calibrationless_mri_reconstruction)

Acknowledgement

This project have been granted by the mobility grant of the SFRMBM and the F society

References I

- Boada, Fernando E. et al. (1997). "Fast three dimensional sodium imaging". In: *Magnetic Resonance in Medicine* 37.5, pp. 706{715.
- Bondell, H.D. and B.J. Reich (2008). "Simultaneous regression shrinkage, variable selection, and supervised clustering of predictors with OSCAR". *Biometrics* 64.1, pp. 115{123.
- Breuer, Felix A et al. (2006). "Controlled aliasing in volumetric parallel imaging (2D CAIPRINHA)". In: *Magnetic Resonance in Medicine* 55.3, pp. 549{556.
- Chandarana, Hersh et al. (2014). "Free-breathing contrast-enhanced T1-weighted gradient-echo imaging with radial k-space sampling for paediatric abdominopelvic MRI". In: *European radiology* 24.2, pp. 320{326.
- Chun, I.Y., B. Adcock, and T.M. Talavage (2016). "Efficient compressed sensing SENSE pMRI reconstruction with joint sparsity promotion". In: *IEEE Transactions on Medical Imaging* 35.1, pp. 354{368.
- Condat, L. (2013). "A primal{dual splitting method for convex optimization involving Lipschitzian, proximable and linear composite terms". *Journal of Optimization Theory and Applications* 158.2, pp. 460{479.

References II

- Friedman, J., T. Hastie, and R. Tibshirani (2010). “A note on the group lasso and a sparse group lasso”. In: *arXiv preprint arXiv:1001.0736*.
- Johnson, Kevin M. et al. (2013). “Optimized 3D ultrashort echo time pulmonary MRI”. In: *Magnetic Resonance in Medicine* 70.5, pp. 1241–1250.
- Lazarus, Carole et al. (2019). “SPARKLING: variable-density k-space filling curves for accelerated T2*-weighted MRI”. In: *Magnetic Resonance in Medicine* 81.6, pp. 3643–3661.
- Majumdar, A.I and R.K. Ward (2012). “Calibration-less multi-coil MR image reconstruction”. In: *Magnetic Resonance in Medicine* 30.7, pp. 1032–1045.
- Roemer, P.B. et al. (1990). “The NMR phased array”. In: *Magnetic Resonance in Medicine* 16.2, pp. 192–225.
- Samsonov, Alexei A et al. (2004). “POCSSENSE: POCS-based reconstruction for sensitivity encoded magnetic resonance imaging”. In: *Magnetic Resonance in Medicine* 52.6, pp. 1397–1406.
- Trzasko, J.D. and A. Manduca (2011). “Calibrationless parallel MRI using CLEAR”. In: *IEEE*, pp. 75–79.

References III

- Uecker, M. et al. (2014). “ESPIRiT– an eigenvalue approach to autocalibrating parallel MRI: where SENSE meets GRAPPA”. In: *Magnetic Resonance in Medicine* 71.3, pp. 990–1001.
- Vũ, BC (2013). “A splitting algorithm for dual monotone inclusions involving cocoercive operators”. In: *Advances in Computational Mathematics* 38.3, pp. 667–681.
- Wang, Zhou et al. (2004). “Image quality assessment: from error visibility to structural similarity”. In: *IEEE transactions on image processing* 13.4, pp. 600–612.